บทความวิจัย

การประเมินพื้นที่เสี่ยงน้ำท่วมภายใต้การเปลี่ยนแปลงสภาพภูมิอากาศ กรณีศึกษา: พื้นที่ราบน้ำท่วม คงเซโดน จังหวัดสาละวัน สปป. ลาว

นิดพอน แสงอะนาทำ
สาขาวิชาการใช้ที่ดินและการจัดการทรัพยากรธรรมชาติอย่างยั่งยืน บัณฑิตวิทยาลัย มหาวิทยาลัยเกษตรศาสตร์
สุดสายสิน แก้วเรือง*
ภาควิชาเกษตรกลวิธาน คณะเกษตร มหาวิทยาลัยเกษตรศาสตร์
พูนศักดิ์ ไม้โภคทรัพย์
ภาควิชาภูมิศาสตร์ คณะสังคมศาสตร์ มหาวิทยาลัยเกษตรศาสตร์
สมฤทัย ทะสดวก
ภาควิชาวิศวกรรมทรัพยากรน้ำ คณะวิศวกรรมศาสตร์ มหาวิทยาลัยเกษตรศาสตร์
วุฒิดา รัตนพิไชย
ภาควิชาปฐพีวิทยา คณะเกษตร มหาวิทยาลัยเกษตรศาสตร์
* ผู้นิพนธ์ประสานงาน โทรศัพท์ 09 6895 1142 อีเมล: agrskr@ku.ac.th
DOI: 10.14416/j.kmutnb.2023.04.001
รับเมื่อ 20 เมษายน 2564 แก้ไขเมื่อ 16 กรกฎาคม 2564 ตอบรับเมื่อ 21 กรกฎาคม 2564 เผยแพร่ออนไลน์ 7 เมษายน 2566

บทคัดย่อ

การวิจัยนี้มีวัตถุประสงค์เพื่อประเมินพื้นที่เสี่ยงน้ำท่วมอันเนื่องจากการเปลี่ยนแปลงสภาพภูมิอากาศ ในพื้นที่ราบน้ำท่วมถึงคงเซโดน จังหวัดสาละวัน สปป. ลาว โดยแบ่งวิธีการศึกษาออกเป็น 5 ส่วนย่อย ได้แก่ 1) การสกัดและการปรับแก้ข้อมูลภูมิอากาศในช่วง ค.ศ. 2020–2100 จากแบบจำลอง Mixed Resolution version of Max Planck Institute Earth System Model (MPI-ESM-MR) ภายใต้การปล่อยก๊าซเรือนกระจกในระดับปานกลาง (RCP4.5) และระดับสูงมาก (RCP8.5) ข้อมูลภูมิอากาศได้ถูกสกัดและปรับแก้ความถูกต้องด้วยแบบจำลอง CMhyd 2) การประเมินปริมาณน้ำท่าในอนาคตภายใต้เงื่อนไข RCP4.5 และ RCP8.5 โดยใช้แบบจำลอง SWAT 3) การวิเคราะห์ขนาดและความถี่ของน้ำท่วมโดยใช้การแจกแจง Log Pearson Type III จากปริมาณน้ำท่าสูงสุดรายปีจากแบบจำลอง SWAT และจากการตรวจวัดในอดีตในช่วง ค.ศ. 1993–2019 ซึ่งปริมาณน้ำท่วมสูงสุดที่คาดว่าจะเกิดขึ้นในอนาคตได้กำหนดรอบปีการเกิดซ้ำที่แตกต่างกัน ได้แก่ รอบ 25, 50, 100 และ 200 ปี 4) การจำลองลักษณะทางชลศาสตร์ เพื่อหาความลึกของน้ำท่วมและความเร็วน้ำท่วม ของแต่ละรอบปีการเกิดซ้ำโดยใช้แบบจำลอง HEC-RAS และ 5) การประเมินระดับพื้นที่เสี่ยงน้ำท่วม โดยใช้หลักการ Flood Hazard Rating (FHR) ด้วยโปรแกรม ArcGIS ผลการศึกษาชี้ให้เห็นว่าพื้นที่เสี่ยงน้ำท่วมเนื่องจากการเปลี่ยนแปลงสภาพภูมิอากาศภายใต้เงื่อนไข RCP4.5 และ RCP8.5 มีแนวโน้มที่จะเพิ่มขึ้น และพื้นที่เสี่ยงน้ำท่วมภายใต้เงื่อนไข RCP8.5 จะสูงกว่า RCP4.5 โดยเฉลี่ยประมาณ 7.44% ค่าความแตกต่างนี้ชี้ให้เห็นว่าการจัดการความเสี่ยงจากน้ำท่วมภายใต้เงื่อนไข RCP8.5 ควรเพิ่มระดับการจัดการมากกว่า RCP4.5 พื้นที่เสี่ยงน้ำท่วมระดับมาก ส่วนใหญ่อยู่บริเวณด้านต้นน้ำและท้ายน้ำ และพื้นที่เสี่ยงปานกลางส่วนใหญ่อยู่บริเวณตอนกลาง ทั้งในเงื่อนไข RCP4.5 และ RCP8.5 ส่วนปริมาณฝนในช่วงฤดูแล้งเพิ่มขึ้น 9.27% (RCP4.5) และ 1.27% (RCP8.5) และช่วงฤดูฝนเพิ่มขึ้น 17.42% (RCP4.5) และ 21.98% (RCP8.5) สำหรับปริมาณน้ำท่าในช่วงฤดูแล้งเพิ่มขึ้น 8.16% (RCP4.5) และ 4.07% (RCP8.5) ส่วนในฤดูฝนเพิ่มขึ้น 13.43% (RCP4.5) และ 18.11% (RCP8.5) ผลที่ได้รับจากการวิจัยครั้งนี้มีประโยชน์อย่างยิ่งในการให้ข้อมูลเบื้องต้นแก่หน่วยงานที่เกี่ยวข้องและคนในชุมชนเพื่อเตรียมรับมือกับเหตุการณ์อุทกภัยโดยเฉพาะการจัดการการใช้ที่ดิน

คำสำคัญ: การสร้างแผนที่เสี่ยงน้ำท่วม การเปลี่ยนแปลงสภาพภูมิอากาศ แบบจำลองทางชลศาสตร์ ระบบสารสนเทศภูมิศาสตร์ ที่ราบน้ำท่วมถึงคงเซโดน

การอ้างอิงบทความ: นิดพอน แสงอะนาทำ, สุดสายสิน แก้วเรือง, พูนศักดิ์ ไม้โภคทรัพย์, สมฤทัย ทะสดวก และ วุฒิดา รัตนพิไชย, "การประเมินพื้นที่เสี่ยงน้ำท่วมภายใต้การเปลี่ยนแปลงสภาพภูมิอากาศ กรณีศึกษา: พื้นที่ราบน้ำท่วม คงเซโดน จังหวัดสาละวัน สปป. ลาว," *วารสารวิชาการพระจอมเกล้าพระนครเหนือ*, ปีที่ 33, ฉบับที่ 3, หน้า 1–13, เลขที่บทความ 233-034973, ก.ค.–ก.ย. 2566.

วารสารวิชาการพระจอมเกล้าพระนครเหนือ ปีที่ 33 ฉบับที่ 3 ก.ค.–ก.ย. 2566
The Journal of KMUTNB., Vol. 33, No. 3, Jul.–Sep. 2023

Research Article

Flood Risk Assessment under Climate Change: Study Case Khongsedon Floodplain, Salavan Province, Lao PDR

Nitphone Senganatham
Sustainable Land Use and Natural Resource Management Program, Graduate School, Kasetsart University, Bangkok, Thailand
Sudsaisin Kaewrueng*
Department of Farm Mechanics, Faculty of Agriculture, Kasetsart University, Bangkok, Thailand
Poonsak Miphokasap
Department of Geography, Faculty of Social Sciences, Kasetsart University, Bangkok, Thailand
Somruthai Tasaduak
Department of Water Resources Engineering, Faculty of Engineering, Kasetsart University, Bangkok, Thailand
Wutthida Rattanapichai
Department of Soil Science, Faculty of Agriculture, Kasetsart University, Bangkok, Thailand

* Corresponding Author, Tel. 09 6895 1142, E–mail: agrskr@ku.ac.th DOI: 10.14416/j.kmutnb.2023.04.001
Received 20 April 2021; Revised 16 July 2021; Accepted 21 July 2021; Published online: 7 April 2023

Abstract

This study aims to assess flood risk areas due to climate change in the Khongsedon floodplain, Salavan province, Lao PDR. The methodology is divided into five subsections: 1) extracting and bias correcting climatic data in the period of A.D. 2020–2100 from MPI-ESM-MR model under moderate greenhouse gas emissions (RCP4.5) and very high greenhouse gas emissions (RCP8.5). The climatic data are extracted and bias corrected by CMhyd model; 2) estimating the future streamflow under RCP4.5 and RCP8.5 using SWAT model; 3) analysis of flood magnitude and frequency using Log Pearson type III distribution of annual maximum streamflow obtained from SWAT model and historical annual maximum streamflow during the period between A.D. 1993–2019. The peak flows were estimated for different return periods such as 25, 50, 100, and 200 years; 4) simulating the hydraulic characteristic s (i.e. flood depth and flood velocity) of each return period using HEC-RAS; and 5) assessment levels of flood prone areas using Flood Hazard Rating (FHR) by ArcGIS. The results indicate that the flood risk areas due to climate change under RCP4.5 and RCP8.5 are more likely to increase, and the flood risk areas under RCP8.5 will be higher than RCP4.5 on average approximately 7.44%. This difference value suggests that under RCP8.5 condition, the degree of management should be greater than the one of RCP4.5. The upper and downstream areas are susceptible to high flood risks while the central area is more likely to experience moderate risks under the RCP4.5 and RCP8.5 conditions. The rainfall in dry season increased by 9.27% (RCP4.5) and 1.27% (RCP8.5). In rainy season, it was found to increase by 17.42% (RCP4.5) and 21.98% (RCP8.5). The dry season streamflow under RCP4.5 and RCP8.5 increased by 8.16% and 4.07%, respectively. In rainy season, runoff increased by 13.43% (RCP4.5) and 18.11% (RCP8.5). The results obtained from this study are particularly useful in providing preliminary information to relevant agencies and people in the community for preparing and dealing with floods events, especially land use management.

Keywords: Flood Risk Mapping, Climate Change, Hydraulic Model, Gis, Khongsedon Floodplain

Please cite this article as: N. Senganatham, S. Kaewrueng, P. Miphokasap, S. Tasaduak, and W. Rattanapichai, "Flood risk assessment under climate change: Study case Khongsedon floodplain, Salavan province, Lao PDR," *The Journal of KMUTNB*, vol. 33, no. 3, pp. 1–13, ID. 233-034973, Jul.–Sep. 2023.

1. Introduction

The Xedon watershed is one of the watersheds, which is affected by climate change as well as other watersheds over the world, and these changes are also sharpened every year. The temperature has increased rapidly and rainfall amount has risen approximately 7% per year [1] consequently, flood events frequently occurred and violent in the Xedon floodplain, particularly in Khongsedon Floodplain (KSF). In early September 2019 the flood events has occurred more severe than the previous years which is unprecedented in this area and it has a huge impact. It resulted in 68 villages affected and 15,300 ha of agricultural area damaged [2]. Therefore, climate change is crucial to be considered in assessing flood risk in the future.

However, the use of the climate change model in assessing the flood risk areas is still not applied extensively, especially in Laos. Most of the previous works have assessed flood risk areas using Flood Magnitude (FLM) that occurred in the past (e.g. Ntanganedzeni and Nobert [3]; Simphaly [4]; Thoummalangsy [5]), the FLM was analyzed by recorded flow data in history. Such a method also has weaknesses because historical flow data may not be consistent with in the future, it will be changed due to climate change conditions. There is a general consensus in the scientific community that climate change has accelerated over the past decades and that climate will continue to change in the future decades [6], this change will impact to the water flow in the future [7]. The Flow due to Climate Change (FLCC) has high importance and influence on the FLM of each return period [8]–[10] that might occur in the future, particularly in case

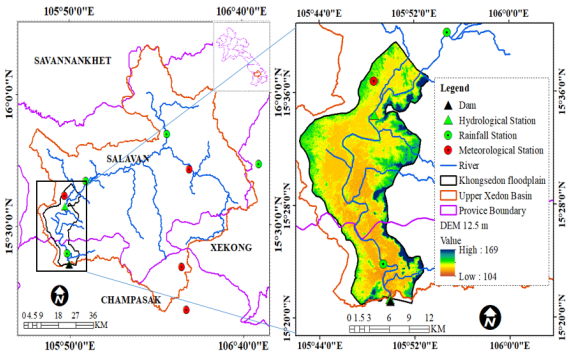

(a) (b)

Figure 1 Study area (a) upper Xedon watershed, (b) Khongsedon Floodplain (KSF).

of the FLCC is greater than the past measurements. Therefore, considering the precipitation or flow data to analyze the FLM of each return period for assessing flood risk areas in the future is extremely important.

In order to fill and solve the gaps mentioned above, this study presents a method for assessing flood risk areas under climate change conditions. The FLMs, that input to assess the flood risk, are obtained from the analysis by the historical flow data recorded from 1993 to 2019 together with future periods due to climate change (i.e. 2020 to 2100) under greenhouse gas emissions (GHGs) of two Representative Concentration Pathways (RCP) scenarios (RCP4.5 and RCP8.5). The climate change data is applied from the Mixed Resolution version of Max Planck Institute Earth System Model (MPI-ESM-MR), which is widely used to investigate the change in climatic parameters and its variability. The objective of this research is to assess flood risk areas due to climate change conditions under RCP4.5 and RCP8.5 in KSF. Its location as depicted in Figure 1 (b).

2. Materials and Methods

2.1 Climate Change Variables Bias Correction

The climate change data that was used for this work include precipitation (*pr*), minimum and maximum temperatures (*tasmin* and *tasmax*) from MPI–ESM–MR, which is widely used to investigate the change in climatic parameters and its variability. MPI–ESM–MR have historical data for the period of 1970 to 2005 and future climatic data under two different scenarios of RCPs (RCP4.5 and RCP8.5) from 2006 to 2100. The RCP4.5 is a trajectory describing radiative forcing of ~4.5 Wm^{-2} (~650 ppm CO_2 eq.) with a stabilization after 2100, corresponding to policies that approximate the mitigation efforts proposed by the governments. The RCP8.5 describes radiative forcing greater than 8.5 Wm^{-2} (~1,370 ppm CO_2 eq.) in 2100. This pathway is seen as a high emission scenario [11], [12].

In this work, the Climate Model data for hydrologic modeling (CMhyd) version 1.02 was used in Extracting (EXT) and Bias Correcting (BC) climate change variables from 2020 to 2100. The CMhyd can be used both for EXT and BC climate change variables that are obtained from Global Circulation Models (GCMs) and Regional Circulation Models (RCMs) [13]. The CMhyd is tailor–made to prepare simulated climate variables for climate change impact studies with the SWAT model [14]. The tool offers several BC methods, including Linear Scaling (LS), Non–Linear Scaling (NLS), and Distribution Mapping (DM) [13]. This work used LS due to it is widely used in adjusting climate data. The bias corrected pr, *tasmin*, and *tasmax* for the future were used as input weather data to SWAT.

$$P_{hst}^{cor}(t) = P_{hst}(t) \times \left[\frac{\mu_m P_{obs}(t)}{\mu_m P_{hst}(t)} \right] \quad (1)$$

$$T_{hst}^{cor}(t) = T_{hst}(t) + \left[\mu_m T_{obs}(t) - \mu_m T_{hst}(t) \right] \quad (2)$$

where, $P_{hst}^{cor}(t)$ and $T_{hst}^{cor}(t)$ are the corrected *pr* and *tasmax* and *tasmin*, respectively; $P_{hst}(t)$ and $T_{hst}(t)$ are the *pr* and *tasmax* and *tasmin* from original climate model outputs during the relevant period; $P_{obs}(t)$ and $T_{obs}(t)$ are the observed *pr* and *tasmax* and *tasmin* in the base year; μ_m denotes the mean value.

2.2 Estimation of Future Streamflow Using SWAT

2.2.1 SWAT inputs data

The SWAT (Soil and Water Assessment Tool) requires physically-based inputs such as topography, land use/land cover (LULC), soil type, and weather data. For topography, we used a 12.5 × 12.5 m Digital Elevation Model (DEM) obtained from the ALOS PALSAR satellite. The LULC data was used in 2015 obtained from the Department of Land Allocation and Development. Soil type data was obtained from Food and Agriculture Organization (FAO). The weather data consist of precipitation, maximum and minimum temperature, relative humidity, solar radiation and wind speed data at daily time intervals for a period of 1993–2019 was obtained from Department of Meteorology and Hydrology. The weather data was prepared by using swat-weather database.

2.2.2 SWAT calibration and validation

The Sequential Uncertainty Fitting (SUFI-2) algorithm within SWAT-CUP was used for model calibration, validation, and sensitivity analysis. SUFI-2 utilizes an objective function to capture the

majority of observed data within a 95% prediction uncertainty (95PPU) in an iterative process [15], [16]. The statistics were used to measure the goodness of fit for the calibrated and validated model viz the coefficient of determination (R^2), Nash-Sutcliffe efficiency (NSE), and Root Mean Square Error ($RMSE$) in Equation 3, 4, 5 respectively. Generally, model simulations are called satisfactory if $R^2 > 0.60$ and $NSE > 0.50$ [9]. One hydrological gauging station, Khongsedon gauging station (H.86), was calibrated and validated. The daily streamflow for the period 1993–2006 was calibrated and the one of period 2007–2019 was validated. After the SWAT model is suitable, the future streamflow under climate change conditions was estimated.

$$R^2 = \frac{N\sum XY - \sum X \sum Y}{\sqrt{N\sum X^2 - \sum X^2} - \sqrt{N\sum Y^2 - \sum Y^2}} \quad (3)$$

$$NSE = 1 - \frac{\sum_{i=1}^{n}(X-Y)^2}{\sum_{i=1}^{n}(X-\bar{X})^2} \quad (4)$$

$$RMSE = \sqrt{\frac{\sum_{i=1}^{n}(X-Y)^2}{N}} \quad (5)$$

where, X is the data from observation; Y is the data from the model; $\bar{X}$ is the mean of data; and N is number of data.

2.3 Flood Magnitude and Frequency Analysis

An analyzed and designed of the frequency of probable flood was determined on the historic annual maximum streamflow during 1993–2019 and the future annual maximum streamflow under climate change conditions for both RCP4.5 and RCP8.5. The period of the future annual maximum streamflow was in 2020-2100. The peak flows were estimated for different return periods such as 25, 50, 100, and 200 years by using Log Pearson type III distribution in Equation (6), which is widely used in design flood magnitude in Lao PDR [17].

$$LogQ(tr) = Log\bar{Q} + K(tr)S(LogQ) \quad (6)$$

where, $LogQ(tr)$ is log of discharge of required return period, $Log\bar{Q}$ is the mean of the logarithms of the annual peak discharges, $K(tr)$ is frequency factor of return period, and $S(LogQ)$ is the standard deviation of the logarithms of the annual peak discharges.

2.4 Extracting the Flood Extent in the Past

In this study, the flood extent as of September 06, 2019 from the Sentinel-1A SAR imagery was extracted in order to use in assessing of performance of the HEC-RAS model in the floodplain areas. The Sentinel-1A belongs to the European Space Agency (ESA) which was launched in 2014. It is a SAR C-band (5.405 GHz) radar satellite. The product format is the Ground Range Detected (GRD) and has a dual polarization, i.e. VV (Vertical transmit and Vertical receive) and VH (Vertical transmit and Horizontal receive). The GRD range azimuth resolution is 20 × 22 m with pixel spacing 10 × 10 m [18]. The imagery of Sentinel-1A SAR was preprocessed by SNAP 7.0. The data processing was composed of seven steps: 1) image subset, 2) applying orbit, 3) thermal noise removal, 4) calibration, 5) speckle filter, 6) terrain correction, and 7) export. Next step

is the preprocessed imagery into QGIS 3.10 for extracting the flood extent. The flood extent was determined from the threshold values of polarization VV and VH. This method is appreciated for its simplicity and low processing time [19], [20].

2.5 Simulating the Future Flood Due to Climate Change

Future flood areas due to climate change under RCP4.5 and RCP8.5 were simulated by HEC-RAS in a one-dimensional (1D) under steady flow conditions (SF). The simulating floods consist of seven steps: 1) digitizing the geometric data (i.e. stream centerline, stream banks, flow paths, and cross sections) employing HEC-GeoRAS. The elevation of geometric data was determined from a DEM 12.5 × 12.5 m, 2) inputting the geometric data into HEC-RAS and then adjusted the bottom depth of the river cross sections to virtual a natural channel bottom because DEM has a limitation of the resolution, it could not see the bottom of the river channel, 3) adding the Manning's roughness coefficient "n" into each the river cross section. The n values were used to be the parameter in calibrating the model, which were depended on type of channel, 4) inputting the flows and setting up the upstream and downstream boundary conditions. In upstream, the flows data from SWAT were inputted because the KSF has no flow gauging station in the upstream. For the flows data period that was inputted in the upstream, the same period that flows data from SWAT and observed at H.86 have a good correlation was selected. The simulation found that a good correlation of flow data between SWAT and observed (H.86) is in January and December of every

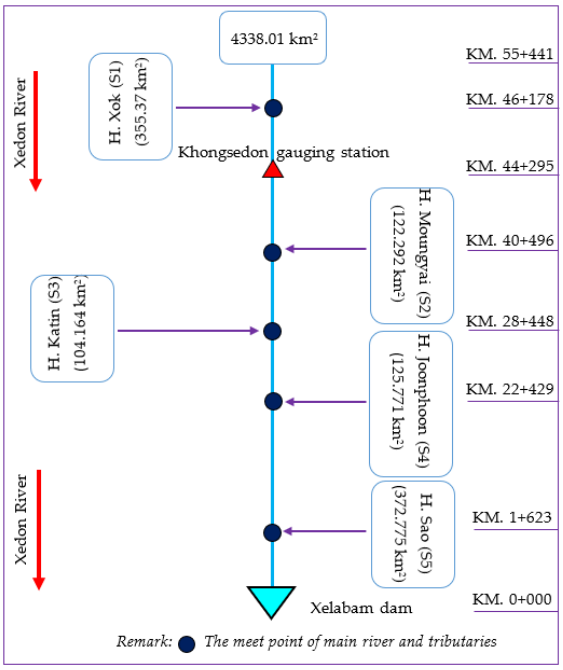

Figure 2 Schematic of the river network in the KSF.

year but this study, the year 2019 was selected. Flow data for the period of January 01–31, 2019 and December 01–31, 2019 was used for calibration and validation, respectively. In the downstream, Xelabam dam (Figure 2), the rating curve was inputted. Apart from this, the flows of lateral inflow obtained from SWAT was inputted. The lateral inflow includes H. Xok (S1), H. Moungyai (S2), H. Katin (S3), H. Joonphoon (S4), and H. Sao (S5), 5) calibrating and validating the river channel at H.86 station by daily flows data. The model performance was assessed using R^2, $RSME$, and Efficiency Index (EI), 6) simulating the flood as September 06, 2019 and then verified the flood extent areas in the floodplain between model and satellite. The model performance in the floodplain was assessed by relative error (RE), and 7) simulating future flood of each return period under climate change conditions.

$$EI = \frac{\sum_{i=1}^{n}\left(X-\bar{X}\right)^2 - \sum_{i=1}^{n}\left(X-Y\right)^2}{\sum_{i=1}^{n}\left(X-\bar{X}\right)^2} \times 100 \quad (7)$$

$$RE = \frac{\left|A_{obs} - A_{\mathrm{mod}}\right|}{A_{obs}} \times 100 \quad (8)$$

where, A_{obs} is flood areas from satellite, and A_{mod} is flood areas from model.

2.6 Assessing Flood Risk Areas

The flood risk area of each return period under RCP4.5 and RCP8.5 was assessed by using the Flood Hazard Rating (FHR) in Equation 9. This equation was proposed by HR Wallingford [21], which is a method for assessing risks to people. The FHR expression chosen for mapping risks to people was:

$$FHR = d \times (v + 0.5) + DF \quad (9)$$

where, FHR is flood hazard rating (m^2/s), d is flood depth from HEC-RAS (m), v is flood velocity from HEC-RAS (m/s), and DF is Debris Factor (= 0, 0.5, 1 depending on the probability that debris will lead to a significantly greater hazard). The flood risk class has divided into four levels including low (FHR < 0.75), moderate (FHR = 0.75–1.25), high (FHR = 1.25–2.5) and extreme (FHR > 2.5) [22].

3. Results

3.1 Changes in Future Climate

As shown in Figure 3, the daily *tasmax* and *tasmin*, and *pr* under RCP4.5 and RCP8.5 are projected to increase for the next 81 years (2020–2100). The *tasmax* and *tasmin* regularly increase. The peak *pr* is expected to occur in 2058 both RCP4.5 and RCP8.5. In the dry season, the 81-year averages of *tasmax* of RCP4.5 and RCP8.5 are 29.9°C and 30.7°C which increases approximately 12.837% and 15.854% as against the baseline (1993–2020) average of 26.5°C. In the rainy season, the *tasmax* of RCP4.5 and RCP8.5 are 29.9°C and 30.7°C which will change 12.7°C and 15.5°C as against the baseline average of 26.6°C. The *tasmin* of RCP4.5 and RCP8.5 in the dry season are 19.6°C and 20.5°C and the percentage change are 8.8°C and 13.9°C compared to the baseline of 18.1°C. In the rainy season, *tasmin* of RCP4.5 and RCP8.5 are 22.4°C and 23.1°C which will change 16.4°C and 19.8°C as against the baseline average of 19.3°C. For the *pr* in the dry season are 458.8 mm (RCP4.5) and 425.4 mm (RCP8.5) which are changed approximately 9.271% and 1.273% for

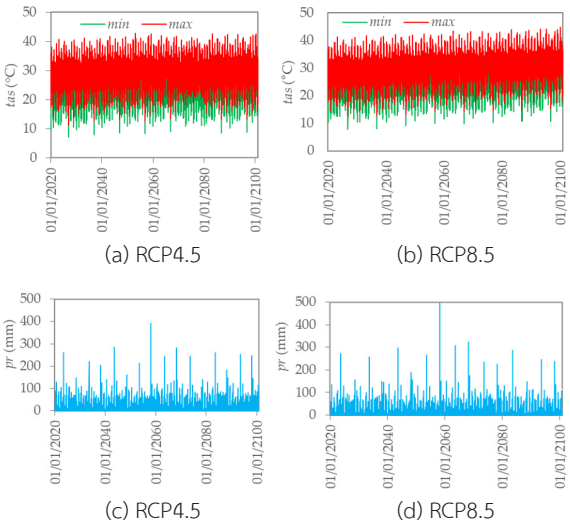

Figure 3 The changing trend of daily *tasmin* and *tasmax* under RCP4.5 (a) and RCP8.5 (b), and *pr* under RCP4.5 (c) and RCP8.5 (d) in the upper Xedon watershed.

RCP4.5 and RCP8.5 as against the baseline average of 420 mm. In the rainy season, the *pr* of RCP4.5 and RCP8.5 are 1,901.6 mm and 1,975.5 mm. The percentage changes are 17.416% (RCP4.5) and 21.980% (RCP8.5) compared to the baseline of 1,619.7 mm. This study, the precipitation and the temperature in the future are expected to increase as projected by the IPCC [23].

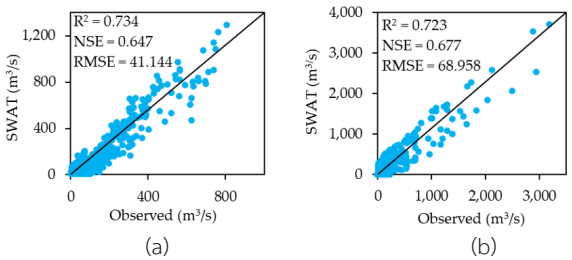

Figure 4 Results of the (a) calibration and (b) validation of daily streamflow at H.86.

3.2 SWAT model results

3.2.1 Calibration and validation results

The daily streamflow was used to analyze the sensitive parameters. These parameters are shown in Table 1. Daily streamflow data from observation at H.86 during the years of 1993–2006 and 2007–2019 were used for calibration and validation, respectively. The model calibration (Figure 4 (a)) and validation (Figure 4 (b)) results imply that the SWAT model performs satisfactorily. It is stated that the calibrated SWAT can be applied to estimate future streamflow due to climate change.

Table 1 Sensitive parameters in SWAT model

Parameters	Used Value	*p*-value
CH_N1	0.035	0.00
CN2	81.50	0.00
CH_N2	0.035	0.01
SOL_K	40.5	0.04
ESCO	0.81	0.07
GW_DELAY	20.00	0.34
SOL_AWC	0.85	0.41
REVAPMN	383.75	0.41
GW_REVAP	0.0136	0.61
RCHRG_DP	0.867	0.75
ALPHA_BF	0.210	0.80
GWQMN	500	0.81

3.2.2 Changes in future streamflow

Changes in seasonal streamflow in two seasons (dry and rainy) at H.86 are projected to increase for the next 81 years (2020–2100), especially in rainy season. In dry season, raises in seasonal streamflow under RCP4.5 and RCP8.5 are 8.16% and 4.07% respectively compared to one of baseline at 3,192,667.33 m^3. In rainy season, RCP4.5 is 13.43% and RCP8.5 is 18.11% against one of baseline at 32,486,715.83 m^3. Streamflow quantities are likely to increase under all RCPs. If this increase, especially in rainy season, is not properly harnessed, flood events will cause impacts on natural, human, and economic at this local.

3.3 Future Flood Return Period

The flood return period analysis were carried out with historic annual maximum streamflow of 1993–2019 and the future annual maximum streamflow under climate change conditions both RCP4.5 and RCP8.5 (2020–2100) by the Log Pearson type III distribution method. The peak discharge is projected to raise under both scenarios, and the peak discharge under RCP8.5 will be higher than RCP4.5 (Table 2). The peak discharge of 100 and 200 years return period under RCP4.5 are similar

to the flood magnitude as of 06 September 2019 (3,174 m^3/s), and the RCP8.5 are 50 and 100 years return period which indicates that the flood in the year 2019 was a huge flood event.

Table 2 The peak discharge of each return period under RCP4.5 and RCP8.5 at H.86

Return Period	Peak Discharge (m^3/s)		Probability (%)
	RCP4.5	RCP8.5	
25	1,672.474	2,237.564	4.0
50	2512.090	2,904.274	2.0
100	2,924.835	3,541.659	1.0
200	3,357.668	4,255.761	0.5

3.4 Flood Extent as of September 06, 2019

The flood extent as of September 06, 2019 in the KSF was extracted from Sentinel-1A SAR imagery. Before extracting the flood extent, the Sentinel-1A SAR imagery was preprocessed by SNAP and then extracted it using QGIS. To identify the flood extent of the preprocessed VV and VH polarization, an approach based on automatic thresholding are chosen. The resulting shows that the flood threshold of polarization $VH \leq 0.008$, $VV \leq 0.005$, and the flood extent is 133.292 km^2. The flood extent as of September 06, 2019 is depicted in Figure 5.

3.5 HEC-RAS Model Results

The Manning's roughness coefficient "n" are calibrated and validated the daily streamflow at H.86. It seem that the suitable "n" for various channel sections is between 0.03 and 0.035. The R^2, EI, and $RMSE$ of calibration and validation are shown in Figure 6. The model calibration and validation in river channel reveals satisfied results.

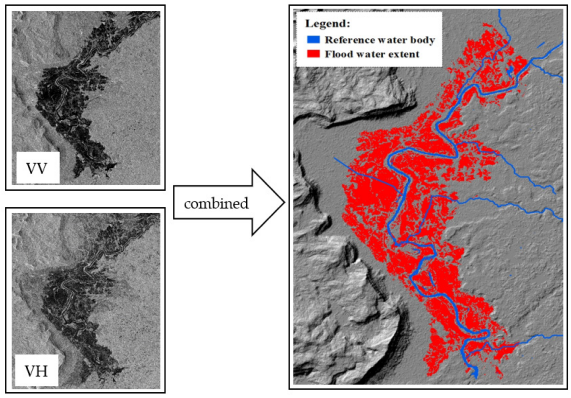

Figure 5 Flood extent extracted on September 06, 2019 from Sentinel-1A.

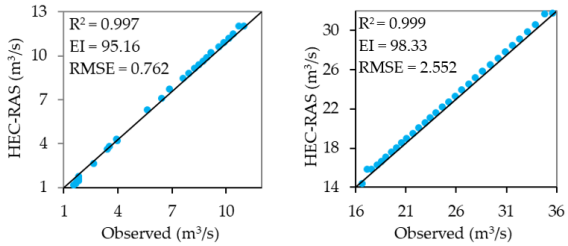

(a) (b)

Figure 6 Results of the (a) calibration for the period of January 01–31, 2019 and (b) validation for the period of December 01–31, 2019 at H.86.

In the floodplain, the flood extent as of September 06, 2019 in the KSF was verified in order to determine the Manning's n for the floodplain of each cross section. The results show the "n" values are between 0.05 and 0.055. The overlap area of flood extent obtained from HEC-RAS and satellite is 102.473 km^2 (Figure 7), which RE equal to 0.07. These results indicate that the model is corresponding to the actual event, therefore the model in part of the floodplain can be applied as well as the river channel part.

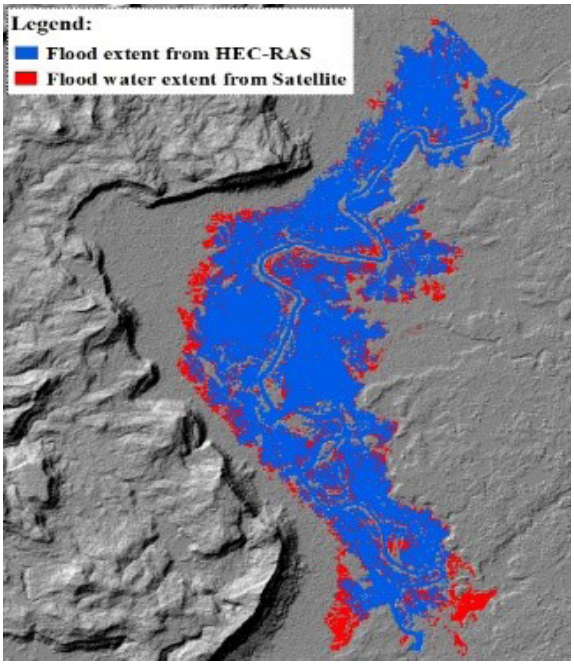

Figure 7 Comparison of the flood extent between HEC-RAS and Satellite as of September 06, 2019.

3.6 Flood Risk Areas Under RCP4.5 and RCP8.5

Future flood risk areas are simulated by using the flood return period under RCP4.5 and RCP8.5 scenarios. The study noticed that the flood risk areas for all return periods under RCP8.5 increasing wider than ones of all return periods under RCP4.5. The maximum flood risk areas under RCP4.5 and RCP8.5 are 126.152 km^2 and 133.722 km^2 respectively. The flood risk areas under RCP4.5 and RCP8.5 scenarios are shown in Table 3 and the flood risk area maps are demonstrated in Figures 8. The villages which will be affected more by serious the risk of flooding in the future under climate change conditions comprising Chanlanxe, Khamko, Nakham, Khongkhoum-Nua, Munpou, Donphaiban, Nahang, Nongboua, Hongluay, Kengtavang, Muangkao, Leung, Nongteng, Hatdou, Nong-Hoy, Tanglang, Na, Kengpho and Nanai.

The land use under various flood risk level was analyzed and found that cropland areas are mostly affected. Subordinate land use are forest, urban and built up, and other land use respectively. Cropland areas are 15.0, 12.709, 22.943 and 64.155 km^2 for low, moderate, high and extreme level respectively. The forest areas are 1.835, 2.087, 2.464 and 8.382 km^2 for low, moderate, high and extreme level respectively. Urban and built up are 0.133, 0.031,

Table 3 Flood risk areas under RCP4.5 and RCP8.5 from various return period in the Khongsedon floodplain

Scenarios	Return Period	Flood Risk Areas (km^2)				
		Low (FHR < 0.75)	Moderate (FHR = 0.75–1.25)	High (FHR = 1.25–2.5)	Extreme (FHR > 2.5)	Total Area
RCP4.5	25	38.172	19.942	19.179	16.703	93.996
	50	25.754	32.028	15.754	40.233	113.768
	100	24.393	29.559	17.571	48.980	120.503
	200	24.107	21.650	23.828	56.567	126.152
RCP8.5	25	28.868	28.389	16.654	34.413	108.324
	50	24.251	29.806	17.559	48.481	120.097
	100	23.157	17.668	26.795	60.050	127.669
	200	17.899	15.503	26.044	74.276	133.722

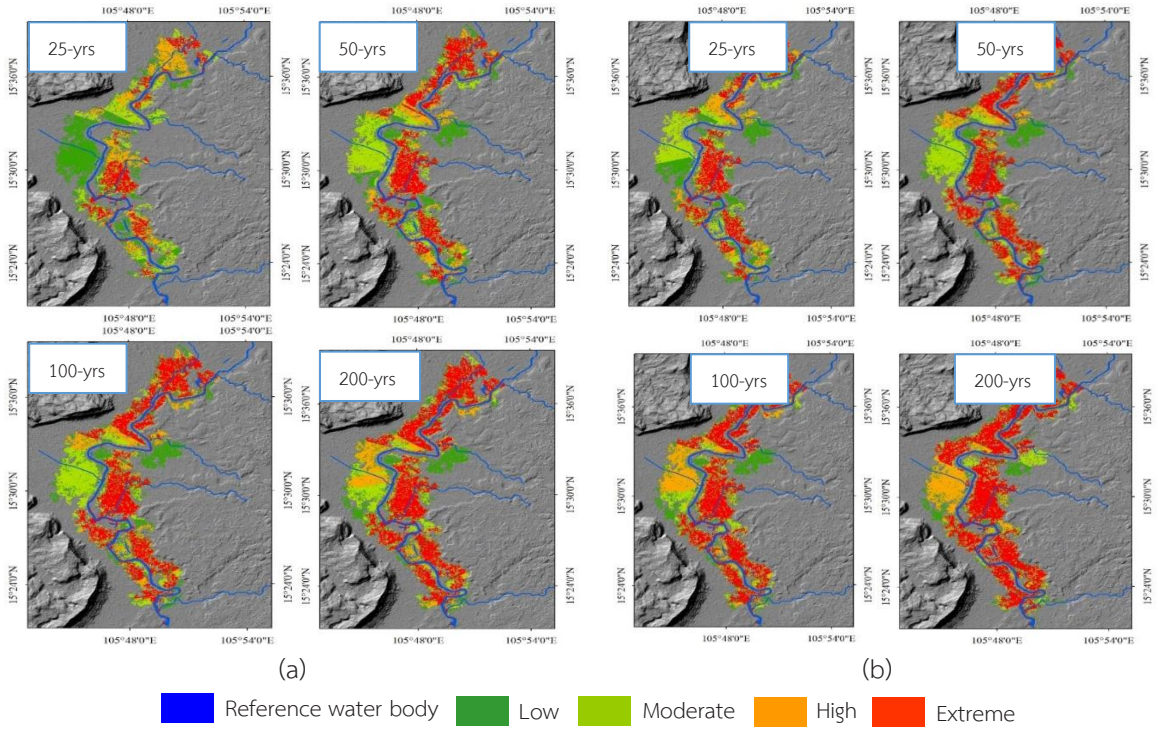

Figure 8 The flood risk areas under (a) RCP4.5 (b) RCP8.5 scenario in the Khongsedon floodplain.

0.022 and 0.177 km^2 for low, moderate, high and extreme level respectively, and other land use at low, moderate, high and extreme are 0.739, 0.526, 0.603 and 11.908 km^2 respectively. It is evident that change in flood risk level influences the area for land use, in particular, croplands which indicate that the agricultural is vulnerable to flooding under climate change.

4. Discussion and Conclusion

In this study, flood risk was assessed by using two climate change conditions like RCP4.5 and RCP8.5 from MPI-ESM-MR at different return periods such as 25, 50, 100, and 200 years. The results of this study reveal the flood magnitude as of September 06, 2019 is nearby the 100 and 200 years return period under RCP4.5 and 50 and 100 years return period under RCP8.5, which indicates that the flood in the year 2019 was a huge flood event. The flood risk areas under RCP4.5 and RCP8.5 will likely increase, and the flood risk areas under RCP8.5 will be higher than one of RCP4.5 by approximately 7.44%. This study presents the guidelines to planners, designers, engineers, and policy-makers in order to deal with the risk of flooding in the future due to climate change conditions. The guideline of community development in the future should avoid the settlement on the flood risk areas of the extreme level if without the preventive measures. This area should be defined as an open space environment, recreation, agriculture, and rural area.

5. Acknowledgements

The authors would like to acknowledge Thailand International Cooperation Agency (TICA) for providing the fund to conduct this research.

References

[1] Ministry of Natural Resources and Environment, "Climate change in Laos yearly 2015," MNRE, Vientiane, Laos, Mar. 2015.

[2] Division of Labour and Social Welfare, "Effects of flood in Khongsedon district, Salavan province in years 2019," DLSW, Vientiane, Laos, Dec. 2019.

[3] B. Ntanganedzeni and J. Nobert, "Flood risk assessment in Luvuvhu river, Limpopo province, South Africa," *Physics and Chemistry of the Earth, Parts A/B/C*, pp. 102959, 2020.

[4] B. Simphaly, "Application of geographic information system for establishing flood map in the Xedon river basin," M.S. thesis, Department of Water Resources Management and Development, Faculty of Water Resources National University of Laos, 2019.

[5] S. Thoummalangsy, "Flood risk assessment for suitable land use management in Xebangfai floodplain, Khammouane province, Lao PDR," M.S. thesis, Sustainable Land Use and Natural Resource Management Program, Graduate School, Kasetsart University, 2019 (in Thai).

[6] M. Parry, M. L. Parry, O. Canziani, J. Palutikof, P. Van der Linden, and C. Hanson, *Climate change 2007-impacts, adaptation and vulnerability: Working group II contribution to the fourth assessment report of the IPCC*. New York: Cambridge University Press, 2007.

[7] A. Watts, G. Grant, and M. Safeeq. (2016, July). Flows of the future—How will climate change affect streamflows in the Pacific Northwest?. United States Department of Agriculture. Portland, USA. [Online]. Available: https://www.fs.fed.us/pnw/sciencef/scifi187.pdf.

[8] X. D. Huang, L. Wang, P. P. Han, and W. C. Wang, "Spatial and temporal patterns in nonstationary flood frequency across a forest watershed: Linkage with rainfall and land use types," *Forests*, vol. 9, no. 6, pp. 339–359, 2018.

[9] M. S. Iqbal, Z. H. Dahri, E. P. Querner, A. Khan, and N. Hofstra, "Impact of climate change on flood frequency and intensity in the Kabul River Basin," *Geosciences*, vol. 8, no. 4, pp. 114–129, 2018.

[10] N. Nyaupane, B. Thakur, A. Kalra, and S. Ahmad, "Evaluating future flood scenarios using CMIP5 climate projections," *Water*, vol. 10, no. 12, pp. 1866–1883, 2018.

[11] J. I. Barredo, G. Caudullo, and A. Mauri, "Mediterranean habitat loss under RCP4. 5 and RCP8. 5 climate change projections," European Commission's science and knowledge service, Luxembourg, 2017.

[12] R. H. Moss, J. A. Edmonds, K. A. Hibbard, M. R. Manning, S. K. Rose, D. P. Van Vuuren, and T. J. Wilbanks, "The next generation of scenarios for climate change research and assessment," *Nature*, vol. 463, no. 7282, pp. 747–756, 2010.

[13] CMhyd user manual, Texas Agricultural Experiment Station and USDA Agricultural Research Service, Washington, D.C, USA, 2016.

[14] B. Zhang, N. K. Shrestha, P. Daggupati, R. Rudra, R. Shukla, B. Kaur, and J. Hou, "Quantifying the impacts of climate change on streamflow dynamics of two major rivers of the Northern Lake Erie Basin in Canada," *Sustainability*, vol. 10, no. 8, pp. 2897–2919, 2018.

[15] *SWAT Calibration and Uncertainty Programs Manual Version 2*, SWAT-CUP2, 2011.

[16] *SWAT Calibration and Uncertainty Programs*, SWAT-CUP, 2008.

[17] V. Kasioudom, *Hydrology*, Vientiane: Faculty of Water Resources, National University of Laos, 2009.

[18] K. Fletcher, *SENTINEL 1: ESA's Radar Observatory Mission for GMES Operational Services*, Paris: European Space Agency, 2012.

[19] P. A. Brivio, R. Colombo, M. Maggi, and R. Tomasoni, "Integration of remote sensing data and GIS for accurate mapping of flooded areas," *International Journal of Remote Sensing*, vol. 23, no. 3, pp. 429–441, 2002.

[20] S. Martinis, A. Twele, and S. Voigt, "Towards operational near real-time flood detection using a split-based automatic thresholding procedure on high resolution TerraSAR-X data," *Natural Hazards and Earth System Sciences*, vol. 9, no. 2, pp. 303–314, 2009.

[21] H.R. Wallingford, "Flooding in boscastle and north cornwall, August 2004. Phase 2 Studies Report," HR Wallingford Limited, Wallingford, UK, Rep. EX5160, 2005.

[22] S. J. Priest, S. M. Tapsell, E. C. Penning-Rowsell, C. Viavattene, and T. Wilson. (2008, June 15). *Building models to estimate loss of life for flood events: executive summary*. [Online]. Available: http://www.floodsite.netFlood.

[23] R. K. Pachauri and L. A. Meyer, "Climate change 2014: synthesis report. Contribution of Working Groups I, II and III to the fifth assessment report of the Intergovernmental Panel on Climate Change," IPCC, Geneva, Switzerland, 2014.